
EIA-SEC: IMPROVED ACTOR-CRITIC FRAMEWORK FOR MULTI-UAV COLLABORATIVE CONTROL IN SMART AGRICULTURE

Quanxi Zhou^{1*}, Wencan Mao^{2*}, Yilei Liang³, Manabu Tsukada¹, Yunling Liu^{4†}, Jon Crowcroft³

¹The University of Tokyo, Tokyo, Japan

²National Institute of Informatics, Tokyo, Japan

³The University of Cambridge, Cambridge, UK

⁴China Agricultural University, Beijing, China

{usainzhou, mtsukada}@g.ecc.u-tokyo.ac.jp, wencan_mao@nii.ac.jp, yl841@cam.ac.uk, jon.crowcraft@cl.cam.ac.uk, yunling@cau.edu.cn.

ABSTRACT

The widespread application of wireless communication technology has promoted the development of smart agriculture, where unmanned aerial vehicles (UAVs) play a multifunctional role. We target a multi-UAV smart agriculture system where UAVs cooperatively perform data collection, image acquisition, and communication tasks. In this context, we model a Markov decision process to solve the multi-UAV trajectory planning problem. Moreover, we propose a novel Elite Imitation Actor-Shared Ensemble Critic (EIA-SEC) framework, where agents adaptively learn from the elite agent to reduce trial-and-error costs, and a shared ensemble critic collaborates with each agent's local critic to ensure unbiased objective value estimates and prevent overestimation. Experimental results demonstrate that EIA-SEC outperforms state-of-the-art baselines in terms of reward performance, training stability, and convergence speed.

Keywords Unmanned Aerial Vehicle, Reinforcement Learning, Actor Critic, and Smart Agriculture.

1 Introduction

The proliferation of digitization technology [1] and the fifth generation of cellular network technology (5G) [2] has boosted the development of smart agriculture [3]. Instead of manually monitoring/analyzing farmland, wireless sensor networks (WSNs) have enabled widespread applications of agricultural data acquisition [4], intelligent monitoring [5], precision agriculture analytics [6], and the implementation of the Agricultural Internet of Things (Agri-IoT) [7].

Meanwhile, the development of unmanned aerial vehicle (UAV) technology has significantly advanced intelligent agriculture [8]. On one hand, UAVs can collect data from WSNs, enabling real-time monitoring of crop growth, efficient data aggregation, and timely environmental analysis [9]. On the other hand, UAVs equipped with cameras can continuously capture aerial imagery of farmland, supporting visual analysis for crop health assessment, pest detection, and disaster monitoring [10]. Moreover, in remote and rugged areas, cellular communication might become inaccessible or be obstructed by obstacles. To address this issue, some UAVs can assist with aerial communication, ensuring reliable information exchange, location sharing, and data aggregation among UAVs without deploying additional ground stations or incurring extra infrastructure costs [11].

In a multi-UAV smart agricultural system, where the UAVs responsible for data collection, image acquisition, and communication co-exist, different types of UAVs are supposed to collaborate with each other while addressing their respective task requirements. Despite heuristics [12], deep reinforcement learning (DRL) [13], hybrid optimization [14],

*The first two authors contributed equally to this work.

†The corresponding author is Yunling Liu (yunling@cau.edu.cn).

and convex optimization [15] have been widely used for trajectory planning for UAVs, there lacks a unified framework for multi-UAV collaborative control in smart agriculture.

However, there are challenges associated with this problem. From a control perspective, each UAV must avoid collision with others [16]. In addition, limited battery capacity and UAV dynamics must be taken into account when making joint decisions, requiring UAVs to adopt energy-efficient strategies [17]. From a communication perspective, UAVs must consider the distance between each other and WSNs to ensure effective information exchange and reliable data transmission [18]. From an application perspective, the quality of information (QoI) metrics include the age of information (AoI) of WSN data collection and visual data freshness (VDF) of image acquisition. If not well planned, competition between UAVs [19] will lead to a reduction in task efficiency and overall QoI performance.

To address the above issues, we propose a *novel elite imitation actor-shared ensemble critic (EIA-SEC)* framework, where each agent is a UAV. To enable agents to learn from high-performing peers with the same type of tasks, we periodically select an elite during training, and allow the actor networks of other agents to softly learn from the actor parameters of the elite agent. This approach reduces trial-and-error costs and guides agents more effectively towards optimal decision directions. As training progresses, agents gradually decrease their reliance on the elite, thereby maintaining exploration and preventing convergence to local optima. In this way, this elite imitation actor (EIA) mechanism improves both the reward performance and the convergence speed of the algorithm, enabling agents to learn effectively and efficiently.

In addition, to ensure the unbiased evaluation of action-state values for each type of task, we equip each agent not only with a local critic, but also with shared ensemble critic (SEC) networks for agents performing the same type of task. During each value evaluation, the local agent critic collaborates with the SEC, contributing to the action-value proportionally. Furthermore, whenever a local critic is updated, the SEC is synchronized accordingly. This mechanism effectively prevents overestimation of Q-values by individual critics, thereby enhancing the stability and convergence of the algorithm. Our key contributions are as follows:

- We target a multi-UAV smart agricultural system, where the UAVs responsible for data collection, image acquisition, and communication tasks co-exist. We construct a Markov decision process (MDP) to tackle the multi-UAV trajectory planning problem for various tasks, considering factors such as AoI, VDF, energy consumption, collision avoidance, and communication quality.
- We propose a *novel EIA-SEC* framework that enhances learning efficiency and stability in multi-agent systems. Agents periodically elect elite individuals, and other agents adaptively learn from their actor parameters to reduce trial-and-error costs. In addition, a shared ensemble critic collaborates with each agent’s local critic to ensure unbiased objective value estimates and prevent overestimation. This combination accelerates convergence, improves performance, and maintains stability in complex collaborative environments.

2 Related Works

UAVs have played increasingly critical roles in intelligent agriculture [20], which range from data collection [21, 22], visual analysis and monitoring [23], and communication [24]. While previous studies focused on a single role, our work considers a multifunctional smart agriculture framework integrating the above functionalities. Furthermore, trajectory planning is a vital research topic for the multi-UAV collaborative system. Traditional methods of UAV trajectory planning include heuristic methods [25], hybrid optimization techniques [26], and convex optimization [27]. Despite their effectiveness in controlled settings, these methods face substantial limitations in real-world applications, such as fixed parameters, high computational complexity, and low adaptation to environmental uncertainty.

Compared with the above algorithms, deep reinforcement learning (DRL) excels in multi-UAV decision-making scenarios. DRL methods, such as deep deterministic policy gradient (DDPG) [28], soft actor-critic (SAC) [29], twin delayed DDPG (TD3) [30], proximal policy optimization (PPO) [31], and counterfactual multi-agent policy gradients (COMA) [32], have been widely used. Furthermore, various modifications and enhancements of DRLs have emerged in recent years. In [33], Randomized Ensemble Double Q-learning (REDQ) was proposed to improve training stability and data efficiency by performing random sampling during updates. However, REDQ relies on extensive environment interactions and requires training and maintaining multiple Q networks, resulting in high computational and memory overhead. In [34], an ensemble learning bootstrapped DQN was designed to leverage the ensemble approach to reduce variance and improve learning stability, but it struggles with the continuous action space tasks and multi-functional agent collaborative systems. In this work, we propose a novel EIA-SEC framework, which enhances learning efficiency and stability in complex, dynamic, and cooperative multi-agent environments.

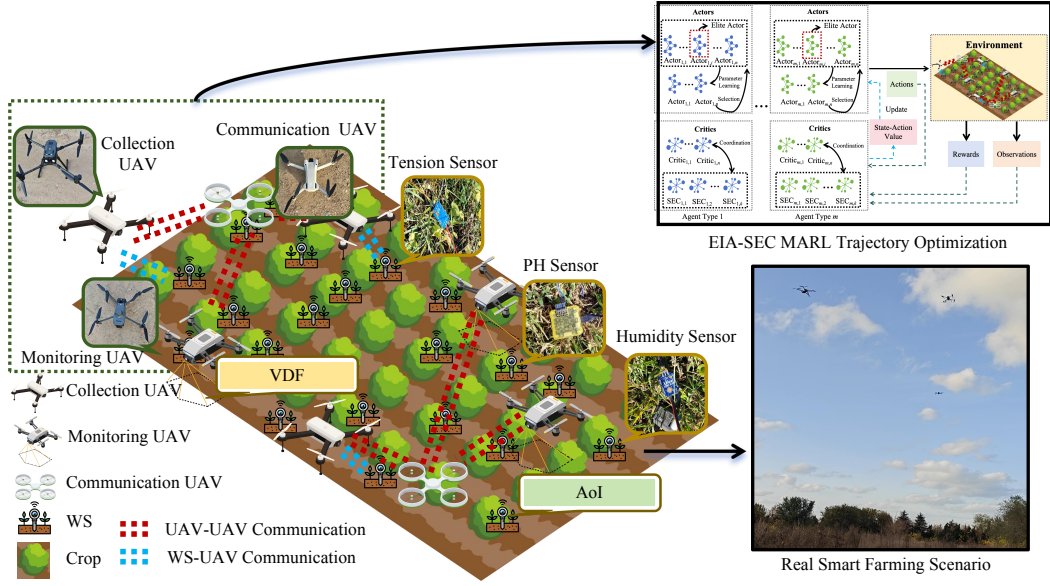


Figure 1: The envisioned multi-UAV collaborative system for smart agriculture, where collection UAVs, monitoring UAVs, and communication UAVs cooperate with each other to minimize the system-level AoI and VDF.

3 System Overview

Fig. 1 demonstrates a collaborative system consisting of n_c communication UAV_c, n_m monitoring UAV_m, and n_d data collection UAV_d to perform smart agricultural tasks. The position of the i -th communication UAV at time t is expressed as $U_c(i, t) = \{U_{cx}(i, t), U_{cy}(i, t), H_{UAV}\}$, where each element represents the coordinates along the x -, y -, and z -axes in the 3D spatial coordinate system, so as the monitoring and data collection UAVs. For each UAV, the 2D task space can be defined as $\mathbb{R}^2 : \{x \in [U_{x-\min}, U_{x-\max}], y \in [U_{y-\min}, U_{y-\max}], H_c | H_m | H_d\}$, where H_c , H_m , and H_d represent the flight height of communication UAV_c, monitoring UAV_m, and data collection UAV_d, respectively. The maximum velocities of the communication, monitoring, and data collection UAVs are assumed to be identical, denoted as $V_{x-\max}$ and $V_{y-\max}$ along the x and y directions, respectively.

The data collection UAVs are responsible for gathering information acquired by the WSN, which consists of multiple categories of wireless sensors (WSs) that are irregularly distributed across the farmland with certain spacing constraints, represented as $WS = \{WS_1, WS_2, \dots, WS_{n_{ws}}\}$. In different farmland scenarios, the distribution of WSs varies with local conditions. Each WS periodically measures soil parameters such as temperature, humidity, and pH level. WSs of different types are configured with distinct data collection and transmission periods depending on their sensing tasks. The freshness of the data is represented by the data AoI, which accumulates over time until out-of-date (i.e., the upper threshold AoI_{\max} is reached).

To obtain real-time images of crop growth and to prevent the intrusion of pests, animals, and birds, the farmland is divided into $n_{px} \times n_{py}$ small plots, which can be represented as $\mathcal{P} = \mathcal{P}_{1,1}, \dots, \mathcal{P}_{n_{px}, n_{py}}$. The monitoring UAVs are responsible for patrolling these plots and capturing image data for each plot area. The freshness of the image information is represented by the VDF, which accumulates over time until out-of-date (i.e., the upper threshold VDF_{\max} is reached).

The communication UAVs are responsible for providing wireless connectivity to both data collection and monitoring UAVs. At each time t , the communication UAVs allocate communication resources to the collaborative multi-UAV system based on the positions of other UAVs and themselves, using the Hungarian algorithm [35]. The communication UAVs maintain real-time inter-UAV communication to aggregate data and positional information received from other UAVs. They perform data analysis and early warning computations. When abnormal situations are detected, the communication UAVs immediately forward the corresponding information to the ground data center (GDC) for further investigations. Meanwhile, they broadcast updated state information, including the status of other UAVs, the system-level AoI, and VDF, to facilitate policy decision-making for other UAVs.

4 System Model

4.1 UAV Communication Model

In the considered scenario, communication UAVs provide communication service for monitoring and collection UAVs. The service protocol can be represented as:

Protocol 1 The communication service protocol

- 1: UAV_m and UAV_d broadcast collected data and positions.
 - 2: UAV_c receives positions and data from UAV_m and UAV_d.
 - 3: UAV_c periodically transmits the aggregated data to GDC.
 - 4: UAV_c determines optimal communication assignments using the Hungarian algorithm as follows:
 - Construct a cost matrix based on link quality and distance between UAV_c and each UAV_m, UAV_d.
 - Find the minimum-cost matching, ensuring efficient and stable connections.
 - Allocate connections according to the optimal assignment results.
 - 5: UAV_c adjusts its position dynamically to maintain high-quality communication links.
-

To improve the service quality of UAV_c, we design a parameter $D_c(i, t)$ to measure the service performance of UAV_{c,i} at time t .

$$D_c(i, t) = \epsilon_1 D_{cg}(i, t) + \epsilon_2 D_{cf}(i, t) + \epsilon_3 D_{cc}(i, t), \quad (1)$$

where $D_{cg}(i, t)$ represents the distance between UAV_{c,i} and the geometric centroid of served UAVs, $D_{cf}(i, t)$ represents the distance between UAV_{c,i} and the farthest served UAV, $D_{cc}(i, t)$ represents the distance between UAV_{c,i} and the geometric centroid of all the communication UAV_c, ϵ_1 , ϵ_2 and ϵ_3 represent the weight coefficients.

4.2 Energy Consumption Model

UAV_c, UAV_m, and UAV_d follow distinct energy consumption models, reflecting their varying operational characteristics.

As for the communication UAV_{c,i}, we set the energy consumption $E_c(i, t)$ as:

$$E_c(i, t) = E_{\text{fly}}(i, t) + E_{\text{comm}}(i, t) + E_{\text{cmp}}(i, t), \quad (2)$$

where $E_{\text{fly}}(i, t)$, $E_{\text{cmp}}(i, t)$, and $E_{\text{comm}}(i, t)$ represent cumulative flight, communication, and computation energy consumption of UAV_i, respectively.

The cumulative flight energy consumption $E_{\text{fly}}(i, t)$ of UAV i at time t can be represented as:

$$E_{\text{fly}}(i, t) = \int_0^t P_{\text{fly}}(i, t) dt, \quad (3)$$

where $P_{\text{fly}}(i, t)$ denotes the instantaneous flight power of UAV_i at time t . The flight power depends on the UAV's aerodynamic structure and velocity, and is expressed as:

$$P_{\text{fly}}(i, t) = \begin{cases} \frac{m_{\text{UAV}} g^{3/2}}{\sqrt{2} \rho_{\text{air}} A_{\text{UAV}} \eta}, & |\mathbf{v}_c(i, t)| < v_{\text{th}}, \\ c_1 |\mathbf{v}_c(i, t)|^2 + \frac{c_2}{|\mathbf{v}_c(i, t)|} + m_{\text{UAV}} g |\mathbf{v}_c(i, t)|, & |\mathbf{v}_c(i, t)| \geq v_{\text{th}}, \end{cases} \quad (4)$$

where m_{UAV} is the UAV mass, g represents the gravitational acceleration, ρ_{air} represents the air density, A_{UAV} represents the frontal area of the UAV, and η denotes the mechanical efficiency. The terms $v_x(i, t)$ and $v_y(i, t)$ correspond to the UAV velocity components along the x and y directions, respectively. A velocity threshold v_{th} is introduced to distinguish between hovering and forward flight, as these states exhibit significantly different power consumption behaviors.

The aerodynamic coefficients c_1 , c_2 , and the frontal area A_{UAV} can be defined as:

$$c_1 = \frac{1}{2} \rho_{\text{air}} A_{\text{UAV}} C_d, \quad (5)$$

$$c_2 = \frac{m_{\text{UAV}}^2}{\eta \rho_{\text{air}} n_{\text{prp}} \pi R_{\text{prp}}^2}, \quad (6)$$

$$A_{\text{UAV}} = A_{\text{surf}} + n_{\text{prp}} \pi R_{\text{prp}}^2, \quad (7)$$

where C_d denotes the air viscosity coefficient, n_{prp} represents the number of propellers, R_{prp} represents the radius of each propeller, and A_{surf} represents the UAV body surface area.

The cumulative UAV computational energy consumption $E_{\text{cmp}}(i, t)$ can be represented as:

$$E_{\text{cmp}}(i, t) = \int_0^t P_{\text{cmp}} dt, \quad (8)$$

where P_{cmp} is a constant representing UAV computational power.

$$P_{\text{cmp}} = P_{\text{static}} + P_{\text{dynamic}}, \quad (9)$$

$$P_{\text{dynamic}} \approx C^* \cdot V^2 \cdot f^* \cdot \alpha^*, \quad (10)$$

where P_{static} represents the static power of the computing module, P_{dynamic} represents the dynamic power of the computing module, C^* represents the load capacitance, V represents voltage, f^* represents clock frequency, and α^* represents the activity factor.

The cumulative UAV communication energy consumption $E_{\text{comm}}(i, t)$ can be represented as:

$$E_{\text{comm}}(i, t) = \int_0^t P_{\text{comm}}(i, t) dt, \quad (11)$$

$$P_{\text{comm}}(i, t) = P_{\text{ut}} + P_{\text{ur}}, \quad (12)$$

where $P_{\text{comm}}(i, t)$ represents the communication power of UAV_{*i*} at time t . P_{ut} is the transmission power from the UAV to the BSs for localization and data transmission, and the second part P_{ur} is transmission power and received signal power at the UAV receiver.

As for the monitoring UAV_{*m,i*}, the energy consumption $E_{\text{m}}(i, t)$ can be represented as:

$$E_{\text{m}}(i, t) = E_{\text{fly}}(i, t) + E_{\text{comm}}(i, t) + E_{\text{cmp}}(i, t) + E_{\text{cam}}(i, t), \quad (13)$$

where $E_{\text{cam}}(i, t)$ represents the camera energy consumption, which can be represented as:

$$E_{\text{cam}}(i, t) = \int_0^t P_{\text{cam}} dt, \quad (14)$$

where P_{cam} represents the camera power.

As for the data collection UAV_{*d,i*}, the energy consumption $E_{\text{d}}(i, t)$ can be represented as:

$$E_{\text{d}}(i, t) = E_{\text{fly}}(i, t) + E_{\text{comm}}(i, t) + E_{\text{cmp}}(i, t) + E_{\text{ec}}(i, t), \quad (15)$$

where $E_{\text{et}}(i, t)$ represents the extra communication energy consumption for data collection, which is represented as:

$$E_{\text{ec}}(i, t) = \int_0^t P_{\text{ec}} dt, \quad (16)$$

where P_{ec} represents the extra communication power.

4.3 Data Collection Model

As a metric reflecting data freshness, the AoI for each WS_{*j*} in the WSN at time t is expressed as $\text{AoI}_j(t)$, defined by

$$\text{AoI}_j(t) = \begin{cases} 0, & \text{if } T_S(j, t) = 1, \\ \text{AoI}_j(t - t_{\text{step}}), & \text{if } T_S(j, t) = 0 \text{ and } t \nmid t_{\text{cycle}} \\ \min\{\text{AoI}_j(t - t_{\text{step}}) + 1, \text{AoI}_{\text{max}}\}, & \text{otherwise,} \end{cases} \quad (17)$$

where $T_S(j, t)$ represents the data transmission success status of WS_{*j*} at time t , t_{cycle} represents the data collection cycle of WS_{*j*}, and t_{step} represents the UAV task time step.

During each update interval $T_{\text{UA}}(i_{\text{type}})$, where i_{type} denotes the WS type index among I_{type} categories, the AoI value increases incrementally. Although WSs of various types differ in their updating intervals $T_{\text{UA}}(i_{\text{type}})$, they share a common AoI upper limit AoI_{max} . At every time slot, each WS_j initiates a connection request broadcast toward nearby UAVs. Upon establishing a connection, WS_j transmits its data packets to the connected UAV_i . If the transmission succeeds, UAV_i replies with an acknowledgment, resetting $\text{AoI}_j(t)$ before the link is released. Otherwise, the transmission attempt times out, and WS_j will retry in the subsequent cycle. Once the data are successfully received, $\text{UAV}_{d,i}$ forwards the aggregated packets to UAV_c through its established communication link. The packet loss rate (PLR) of $\text{UAV}_{d,i}$ during transmission can be modeled as:

$$\text{PLR}(U_d(i, t)) = 1 - (1 - \text{BER}(U_d(i, t)))^L, \quad (18)$$

where L is the packet length, and $\text{BER}(U_d(i, t))$ denotes the bit error rate at location $U_i(t)$. As binary phase shift keying (BPSK) modulation is applied, the $\text{BER}(U_d(i, t))$ is given by

$$\text{BER}(U_d(i, t)) = Q\left(\sqrt{2 \cdot \text{SINR}(U_d(i, t))}\right), \quad (19)$$

where $\text{SINR}(U_d(i, t))$ is the signal-to-interference-plus-noise ratio (SINR) at position $U_d(i, t)$, and $Q(x)$ represents the Q -function in communication theory, defined as

$$\text{SINR}(U_d(i, t)) = \frac{\sum_{k, \text{WS}_k \in \text{WS}} P_{\text{WT}}(t) + G_{\text{WS}}(t) - PL(i, j, t)}{\sum_{k, \text{WS}_k \notin \text{WS}} P_{\text{WT}}(t) + G_{\text{WS}}(t) - PL(i, j, t) + P_{\text{T}}}, \quad (20)$$

$$Q(x) = \frac{1}{\sqrt{2\pi}} \int_x^\infty e^{-\frac{t^2}{2}} dt \approx \frac{1}{2} e^{-\frac{x^2}{2}}, \quad (21)$$

where $P_{\text{WT}}(t)$ denotes the transmission power of WSs, $G_{\text{WS}}(t)$ is the antenna gain, $PL(i, j, t)$ represents the propagation path loss between UAV_i and WS_j , and P_{T} is the thermal noise power defined by

$$P_{\text{T}} = k_B \times T_K \times Bw, \quad (22)$$

where k_B is Boltzmann's constant, T_K is the absolute temperature in Kelvin, and Bw denotes the communication bandwidth. The total path loss $PL(i, j, t)$ between $\text{UAV}_{d,i}$ and WS_j can be expressed as

$$PL(i, j, t) = PL_{\text{FS}}(\text{Dis}(i, j, t), f_c) + PL_{\text{veg}}(\text{Dis}(i, j, t), f_c), \quad (23)$$

$$PL_{\text{FS}}(\text{Dis}(i, j, t), f_c) = 20 \log_{10}(\text{Dis}(i, j, t)) + 20 \log_{10}(f_c) + 32.44, \quad (24)$$

$$PL_{\text{veg}}(\text{Dis}(i, j, t), f_c) = a_1 f_c^{a_2} \text{Dis}(i, j, t)^{a_3}, \quad (25)$$

where $\text{Dis}(i, j, t)$ indicates the distance between $\text{UAV}_{d,i}$ and WS_j at time t , f_c is the carrier frequency, $PL_{\text{FS}}(\cdot)$ is the free-space path loss, and $PL_{\text{veg}}(\cdot)$ is the vegetation-induced path loss [36]. Parameters a_1 , a_2 , and a_3 denote the scaling factor, frequency exponent, and distance exponent, respectively.

4.4 Monitoring Model

To facilitate statistics, the farmland is divided into $n_{px} \times n_{py}$ small plots, which can be represented as $\mathcal{P} = \mathcal{P}_{1,1}, \dots, \mathcal{P}_{n_{px}, n_{py}}$, as mentioned in Section 3. The monitoring UAVs are responsible for patrolling these plots and capturing image data for each grid area. To facilitate the computation and assessment of UAV image quality, each plot is divided into $n_{gx} \times n_{gy}$ grids, which can be represented as $G = G_{0,0}, G_{0,1}, \dots, G_{n_{gx}, n_{gy}}$. The image quality of each grid is determined based on the UAV's distance and viewing angle relative to the grid. The overall image quality of the plot is then obtained by aggregating the evaluation of all grids. Assume that the distance between grid $G_{x', y'}$ and the closest UAV can be denoted as $d_G(x', y')$. We define a distance threshold d_{th} . If the actual average distance $d_G(x', y')$ exceeds d_{th} (i.e., $d_G(x', y') > d_{\text{th}}$), the image quality is considered poor; otherwise, it is deemed acceptable. The image quality of grid $G_{x', y'}$ can be denoted as $\mathcal{Q}(x', y', t)$, which can be represented as

$$\mathcal{Q}(x', y', t) = \begin{cases} 0, & \text{if } d_G(x', y') < d_{\text{th}}, \\ 1, & \text{Otherwise.} \end{cases} \quad (26)$$

In this context, the image quality $\mathcal{Q}_{\text{plot}}(x, y, t)$ of the whole monitoring plot $\mathcal{P}_{x,y}$ at time t can be represented as

$$\mathcal{Q}_{\text{plot}}(x, y, t) = \frac{\sum_{x'=0}^{n_{gx}} \sum_{y'=0}^{n_{gy}} \mathcal{Q}(x', y', t)}{n_{gx} \cdot n_{gy}}, \quad (27)$$

We define a lowest acceptable quality threshold \mathcal{Q}_{th} for $\mathcal{Q}_{\text{plot}}(x, y, t)$ to be deemed successful. The Monitoring success metric $V_S(x, y, i, t)$ of UAV_{m,i} in plot $\mathcal{P}_{x,y}$ at time t can be represented as

$$V_S(x, y, i, t) = \begin{cases} 0, & \text{if } \mathcal{Q}_{\text{plot}}(x, y, t) < \mathcal{Q}_{\text{th}}, \\ 1, & \text{Otherwise.} \end{cases} \quad (28)$$

As a metric reflecting visual data freshness, the VDF, UAV_{m,i} visiting, for each plot $\mathcal{P}_{x,y}$ at time t is expressed as $\text{VDF}_{x,y}(i, t)$, defined by

$$\text{VDF}_{x,y}(i, t) = \begin{cases} 0, & \text{if } \mathcal{Q}_{\text{plot}}(x, y, t) \geq \mathcal{Q}_{\text{th}}, \\ \text{VDF}_{x,y}(t - t_{\text{step}}), & \text{if } \mathcal{Q}_{\text{plot}}(x, y, t) < \mathcal{Q}_{\text{th}} \text{ and } t \nmid t_v, \\ \min\{\text{VDF}_{x,y}(t - t_{\text{step}}) + 1, \text{VDF}_{\text{max}}\}, & \text{otherwise,} \end{cases} \quad (29)$$

where t_v represents the VDF update cycle.

5 Design of EIA-SEC

5.1 Markov Decision Process

5.1.1 Agent

In the considered scenario, each agent is a UAV that makes its own decision. Assume that the agent represents the communication UAV_c as $\{\text{agent}_{c,1}, \dots, \text{agent}_{c,n_c}\}$, monitoring UAV_m as $\{\text{agent}_{m,1}, \dots, \text{agent}_{m,n_m}\}$, and UAV_d as $\{\text{agent}_{d,1}, \dots, \text{agent}_{d,n_d}\}$.

5.1.2 Observation of Each Agent

In the intelligent farming scenario, UAV_c, UAV_m and UAV_d have distinct observation spaces. As for UAV_c, the observation space should provide information on the UAV_c position $\mathcal{U}_c(i, k)$; the distance $d_{C-c}(i, k)$ and coordinates UAV_{C-c}(i, k) of the nearest communication UAV; the geometric center $\text{GC}_c(i, k)$ of the UAV_c, and its distance $d_{\text{GC-c}}(i, k)$ to the geometric center; the geometric center $\text{GC}_u(i, k)$ of the served UAV swarm, and its distance $d_{\text{GC-u}}(i, k)$ to the geometric center; and the distance $d_{f-s}(i, k)$ and coordinates UAV_{f-s}(i, k) of the farthest served UAV; the nearest UAV_{N}(i, k) and the distance $d_U(i, k)$ between them.}}}

$$\mathbf{o}_{c-i,k} = \{\mathcal{U}_c(i, k), \text{UAV}_{C-c}(i, k), d_{C-c}(i, k), \text{GC}_c(i, k), d_{\text{GC-c}}(i, k), \text{GC}_u(i, k), d_{\text{GC-c}}(i, k), \text{UAV}_{f-s}(i, k), d_{f-s}(i, k), \text{UAV}_N(i, k), d_U(i, k)\}, \quad (30)$$

As for UAV_m, the observation space should provide information on UAV position $\mathcal{U}_m(i, k)$; the VDF information $\{\text{VDF}_{x-1,y-1}(i, k), \dots, \text{VDF}_{x+1,y+1}(i, k)\}$ around the plot $\mathcal{P}_{x,y}$, where UAV_{m,i} is flying; the direction $D_{\text{VDF}}(i, k)$ of the quadrant with the highest VDF concentration; the nearest UAV_{N}(i, k) and the distance $d_U(i, k)$ between them.}

$$\mathbf{o}_{i,k} = \{\mathcal{U}_m(i, k), \text{VDF}_{x-1,y-1}(i, k), \dots, \text{VDF}_{x+1,y+1}(i, k), D_{\text{VDF}}(i, k), \text{UAV}_N(i, k), d_U(i, k)\}, \quad (31)$$

As for UAV_d, the observation space should provide information on UAV position $\mathcal{U}_d(i, k)$; the AoI information of nearby WSs $\{\text{AoI}(i, j_1, k), \dots, \text{AoI}(i, j_n, k)\}$; the direction $D_{\text{AoI}}(i, k)$ of the quadrant with the highest AoI concentration; the nearest UAV_{N}(i, k) on the same flight plane and the distance $d_U(i, k)$ between them.}

$$\mathbf{o}_{i,k} = \{\mathcal{U}_d(i, k), \text{AoI}(i, j_1, k), \dots, \text{AoI}(i, j_n, k), D_{\text{AoI}}(i, k), \text{UAV}_N(i, k), d_U(i, k)\}, \quad (32)$$

5.1.3 Action of Each Agent.

Action space of UAV_c, UAV_m, and UAV_d are the same, all consist of the flying speed vector

$$\mathbf{a}_{c-i,k} = \{v_{c-x}(i, k), v_{c-y}(i, k)\}, \quad (33)$$

$$\mathbf{a}_{m-i,k} = \{v_{m-x}(i, k), v_{m-y}(i, k)\}, \quad (34)$$

$$\mathbf{a}_{d-i,k} = \{v_{d-x}(i, k), v_{d-y}(i, k)\}, \quad (35)$$

where the speed in x and y direction are within $V_{x-\text{max}}$ and $V_{y-\text{max}}$, respectively.

5.1.4 Reward of Each Agent $r_{c-i,k}$, $r_{m-i,k}$, and $r_{d-i,k}$

The reward is the feedback provided by the environment to agents based on their observation and chosen action.

As for communication UAVs, we consider to maximize the quality of the communication service UAV_c providing for UAV_m and UAV_d while minimizing waste of resources, boundary violation and collision risk penalties.

To ensure that the communication UAV_{c,i} can provide reliable communication services for other task UAVs, we design a communication positioning function $DPF_{C-i}(t)$ based on the relative positions of the UAVs, which is represented as

$$DPF_{C-i}(t) = \int_0^t D_c(i, t) dt = \sum_{k=0}^{k_t} (D_c(i, k+1) - D_c(i, k)) \cdot t_{\text{step}}. \quad (36)$$

The total energy consumption $E_{C-i}(t)$ of i -th UAV can be denoted as:

$$E_{C-i}(t) = E(i, t) \approx \sum_{k=0}^{k_t} (E(i, k+1) - E(i, k)) \cdot t_{\text{step}}. \quad (37)$$

To avoid collisions with each other, a safety risk penalty $D_{U-i}(t)$ is set to describe the collision risk between UAV_{c,i} and other UAVs. It can be represented as:

$$D_{U-i}(t) = \int_0^t SR(i, t) dt = \sum_{k=0}^{k_t} SR(i, k) \cdot t_{\text{step}} \quad (38)$$

$$SR(i, t) = \begin{cases} d_U(i, t) - d_U(i, t - t_{\text{step}}), & d_U(i, t) < d_{\text{safety}}, \\ 0, & \text{otherwise,} \end{cases} \quad (39)$$

$$d_{\text{safety}} = 2 \cdot \sqrt{(V_{x-\text{max}}^2 + V_{y-\text{max}}^2)}, \quad (40)$$

where $d_U(i, t)$ represents the distance between i -th UAV and the closest UAV_N(i, t) at time t , $SR(i, t)$ represents the safety risks of UAV collisions, and d_{safety} is the safety threshold.

Besides, to avoid UAV_i flying out task space, a boundary violation penalty $\mathcal{P}_{O-i}(t)$ is set as:

$$\mathcal{P}_{O-i}(t) = \int_0^t ACT(i, t) dt = \sum_{k=0}^{k_t} ACT(i, k) \cdot t_{\text{step}}, \quad (41)$$

$$ACT(i, t) = \begin{cases} 1, & \text{out of range,} \\ 0, & \text{otherwise,} \end{cases} \quad (42)$$

where $ACT(i, t)$ represents the area compliance tracking of i -th UAV at time t .

The communication UAV reward can be represented as

$$r_{c-i,k} = [\alpha_1(D_c(i, k) - D_c(i, k-1)) - \alpha_2(E(i, k) - E(i, k-1)) - \alpha_3 SR(i, k) - \alpha_4 ACT(i, k)] \cdot t_{\text{step}}. \quad (43)$$

As for monitoring UAVs, we consider maximizing the quality of the monitoring task of UAV_m while minimizing waste of resources, boundary violations, collision risks, and capture failure penalties.

To motivate the UAVs to capture efficiency, we describe visual monitoring utility value VMUF(i, t) as

$$VMUF(i, t) = \int_0^t VDF_{x,y}(i, t) \cdot V_S(x, y, i, t) dt, \quad (44)$$

To evaluate the quality of monitoring of UAV_{m,i}, we define a VDF penalty $\mathcal{P}_M(i, t)$ as

$$\mathcal{P}_M(i, t) = \begin{cases} 1, & \text{if VMUF}(i, t) = 0, \\ 0, & \text{otherwise.} \end{cases} \quad (45)$$

To ensure the trend of efficient monitoring, we define a VDF motivation $\mathcal{M}_V(i, t)$ as

$$\mathcal{M}_V(i, t) = \begin{cases} 1, & \text{if } \arccos\left(\frac{\mathbf{v}_m(i, t) \cdot D_{\text{VDF}}(i, t)}{\|\mathbf{v}_m(i, t)\| \|D_{\text{VDF}}(i, t)\|}\right) < 90^\circ, \\ 0, & \text{otherwise} \end{cases}, \quad (46)$$

We design the $r_{m-i, k}$ as

$$r_{m-i, k} = [-\alpha_2(E(i, k) - E(i, k - 1)) - \alpha_3 SR(i, k) - \alpha_4 ACT(i, k) + \alpha_5 \text{VMUF}(i, k) - \alpha_6 \mathcal{P}_M(i, k) + \alpha_7 \mathcal{M}_V(i, k)] \cdot t_{\text{step}}. \quad (47)$$

As for data collection UAVs, we consider to maximize utility value of collected data of UAV_d while minimizing waste of resources, boundary violation, collision risk, and waste of resources penalties.

To motivate the UAVs to collect rich and up-to-date data, we denote the data collection utility function DCUF(i, t) as

$$\text{DCUF}(i, t) = \int_0^t \text{AoI}(i, j, t) \cdot T_S(i, j, t) dt, \quad (48)$$

where AoI(i, j, t) denotes the AoI of WS_{*j*} that UAV_{d, *i*} collects at time t and $T_S(i, j, t)$ represents the data transmission success status function.

To evaluate the quality of data collection of UAV_{d, *i*}, we define an AoI penalty $\mathcal{P}_C(i, t)$ as

$$\mathcal{P}_C(i, t) = \begin{cases} 1, & \text{if } \text{DCUF}(i, t) = 0, \\ 0, & \text{otherwise,} \end{cases} \quad (49)$$

We define an AoI motivation $\mathcal{M}_d(i, t)$ as

$$\mathcal{M}_d(i, t) = \begin{cases} 1, & \text{if } \arccos\left(\frac{\mathbf{v}_d(i, t) \cdot D_{\text{AoI}}(i, t)}{\|\mathbf{v}_d(i, t)\| \|D_{\text{AoI}}(i, t)\|}\right) < 90^\circ, \\ 0, & \text{otherwise} \end{cases}, \quad (50)$$

We design the $r_{d-i, k}$ as

$$r_{d-i, k} = [-\alpha_2(E(i, k) - E(i, k - 1)) - \alpha_3 SR(i, k) - \alpha_4 ACT(i, k) + \alpha_8 \text{DCUF}(i, k) - \alpha_9 \mathcal{P}_C(i, k) + \alpha_{10} \mathcal{M}_D(i, k)] \cdot t_{\text{step}}. \quad (51)$$

5.2 Elite Imitation Actor

To expedite the training process and enable agents to leverage the behavioral patterns of high-performing individuals, we introduce an elite imitation mechanism. This mechanism is formulated to mitigate prolonged low-reward exploration by guiding agents toward more effective behavioral trajectories observed in the selected elite.

We encourage agents belonging to the same category to learn from one another. Let agent_{*v*} denote a generic agent category that shares comparable behavioral patterns and underlying task structures, which enables more effective intra-category knowledge transfer, where $v = \{c, m, d\}$. We introduce a mimicry cycle factor, denoted by δ_v . During certain episodes determined by this factor, each agent_{*v-i*} temporarily suspends the direct update of its policy network $\pi_{v-i}(\theta_{v-i})$. The agent generates an action sequence $\mathcal{A}_{v-i} = \{a_{v-i, 0}, a_{v-i, 1}, \dots, a_{v-i, n_v}\}$ and interacts with the environment to obtain a corresponding reward vector $\mathcal{R}_{v-i} = \{r_{v-i, 1}, r_{v-i, 2}, \dots, r_{v-i, n_v}\}$, where n_v represents the number of agent_{*v*}.

The elite policy is then identified based on the mean μ_{v-i} and variance σ_{v-i}^2 of the rewards in \mathcal{R}_{v-i} . To quantify the performance of agent_{*v-i*}, we define an evaluation metric as:

$$\omega_{v-i} = \beta_1 \mu_{v-i} + \beta_2 \sigma_{v-i}^2. \quad (52)$$

Specifically, we select the agent_{*v-i'*} with the best-performing reward profile as the elite individual. Subsequently, the remaining agents update their policy networks through a soft imitation process, where parameters are softly copied from the elite policy using a soft update coefficient ϑ . The update rule is formulated as:

$$\theta_{v-i} = (1 - \vartheta)\theta_{v-i} + \vartheta\theta_{v-i'}, \quad (53)$$

where $\theta_{v-i'}$ and θ_{v-i} denote the parameters of the elite and agents' policy networks, respectively. Furthermore, to preserve a certain level of exploration while leveraging the elite imitation strategy, we progressively adjust the influence of the imitation process over time. Specifically, the soft update coefficient ϑ is gradually decreased, whereas the mimicry cycle factor δ is progressively increased. We initialize these parameters as ϑ^* and δ^* , respectively. The detailed procedure of the proposed algorithm is presented in **Algorithm 2**.

Algorithm 2 Elite Imitation Actor Mechanism

```

1: Initialize policy network  $\pi_{v-i}(\theta_{v-i})$  for each agent $_{v-i}$ .
2: Initialize  $\vartheta \leftarrow \vartheta^*$  and  $\delta \leftarrow \delta^*$ .
3: for episode  $\lambda = 1, 2, \dots, \lambda_{\max}$  do
4:   if  $\lambda \mid \delta$  then
5:     for agent $_{v-i}$   $i = 1, 2, \dots, n_v$  do
6:       Generate  $\mathcal{A}_{v-i}$  from  $\pi_{v-i}(\theta_{v-i})$ .
7:       Obtain Reward  $\mathcal{R}_i$  from the interaction between agent $_{v-i}$  and the environment.
8:     end for
9:     Compute the maximum reward evaluation parameter  $\omega_{v-i}$  as Equation (52).
10:    Update  $\pi_{v-i}(\theta_{v-i})$  as Equation (53).
11:    Update parameters  $\vartheta \leftarrow \frac{1}{2}\vartheta$  and  $\delta \leftarrow 2\delta$ .
12:  end if
13: end for

```

5.3 Shared Ensemble Critic

To enable the critics to provide more impartial evaluations of action-state values, we introduce the SEC mechanism. Similarly, we define agent $_v$ as a generic category of agents that share behavioral patterns and underlying task structures, thereby facilitating more effective intra-category knowledge transfer, where $v = \{c, m, d\}$. The SEC mechanism ensures that each agent $_{v-i}$ is equipped with its own independent critic $\mathcal{Q}_{v-i}(\phi_{v-i})$ and target critic, $\mathcal{Q}'_{v-i}(\phi'_{v-i})$, while a shared ensemble of critics $\mathcal{Q}_{s,v}(\phi_s) = \{\mathcal{Q}_{s,v-1}(\phi_{s-1}), \dots, \mathcal{Q}_{s,v-k_s}(\phi_{s,v-k_s})\}$ is additionally constructed for the entire agent $_v$ category to enhance stable value estimation across agents.

Assuming that during the update, $R_{B,v-i}$ represents a batch size of reward from agent $_{v-i}$, the target value can be represented as:

$$\mathcal{Y} = R_{B,v-i} + \gamma \cdot \mathcal{Q}'_{v-i}(\phi'_{v-i}) \quad (54)$$

where γ represents the discount rate.

Then we define the predicted Q-value $\mathcal{Q}_{P,v-i}$ as:

$$\mathcal{Q}_{P,v-i} = \epsilon \cdot \mathcal{Q}_{v-i}(\phi_{v-i}) + (1 - \epsilon) \cdot \left(\sum_{k=0}^{k_s} \frac{\mathcal{Q}_{s,v-k}(\phi_{s-k})}{k_s} \right) \quad (55)$$

where ϵ represents the rate parameter. We minimize the mean squared error (MSE) between the predicted Q-values and target Q-values. We update the critic and SEC networks by minimizing the loss function $\mathcal{J}_{\mathcal{Q}}(\phi_{v-i})$:

$$\mathcal{J}_{\mathcal{Q}_{v-i}}(\phi_{v-i}) = \mathcal{J}_{\mathcal{Q}_{s,v-k}}(\phi_i) = \mathbb{E}[(\mathcal{Q}_{P,v-i} - \mathcal{Y})^2], \quad (56)$$

where $\mathbb{E}(\cdot)$ represents the the mathematical expectation.

Moreover, to ensure sufficient diversity among the ensemble members, we proportionally replicate the parameters of the Q-networks within the SEC as

$$\phi_{s,v-k} = \frac{\tau k}{k_s} \phi_{v-i} + \left(1 - \frac{\tau k}{k_s}\right) \phi_{s,v-k}, \quad (57)$$

where τ represents the parameter rate. Also, we will softly update the target critic networks toward the current critic networks to ensure training stability. Instead of directly copying the weights, the target networks are updated using a weighted average of the current and previous target weights:

$$\phi'_{v-i} = \xi \phi_{v-i} + (1 - \xi) \phi'_{v-i} \quad (58)$$

where ξ is the soft update parameter.

The detailed procedure of proposed algorithm is presented in **Algorithm 3**.

Algorithm 3 Shared Ensemble Critics Mechanism

- 1: Initialize critic network $Q_{v-i}(\phi_{v-i})$ for each agent $v-i$.
- 2: Initialize $Q_{s,v}(\phi_s) = \{Q_{s,v-1}(\phi_{s-1}), \dots, Q_{s,v-k_s}(\phi_{s,v-k_s})\}$.
- 3: **for** episode $\lambda = 1, 2, \dots, \lambda_{\max}$ **do**
- 4: **for** agent $v-i = 1, 2, \dots, n_v$ **do**
- 5: Generate action by policy network $\pi_{v-i}(\theta_{v-i})$.
- 6: Evaluate the action-state value by (55).
- 7: Update $Q_{v-i}(\phi_{v-i})$ by (56).
- 8: Update $Q_{s,v}(\phi_s)$ by (57).
- 9: Softly update $Q'_{v-i}(\phi'_{v-i})$ by (58).
- 10: **end for**
- 11: **end for**

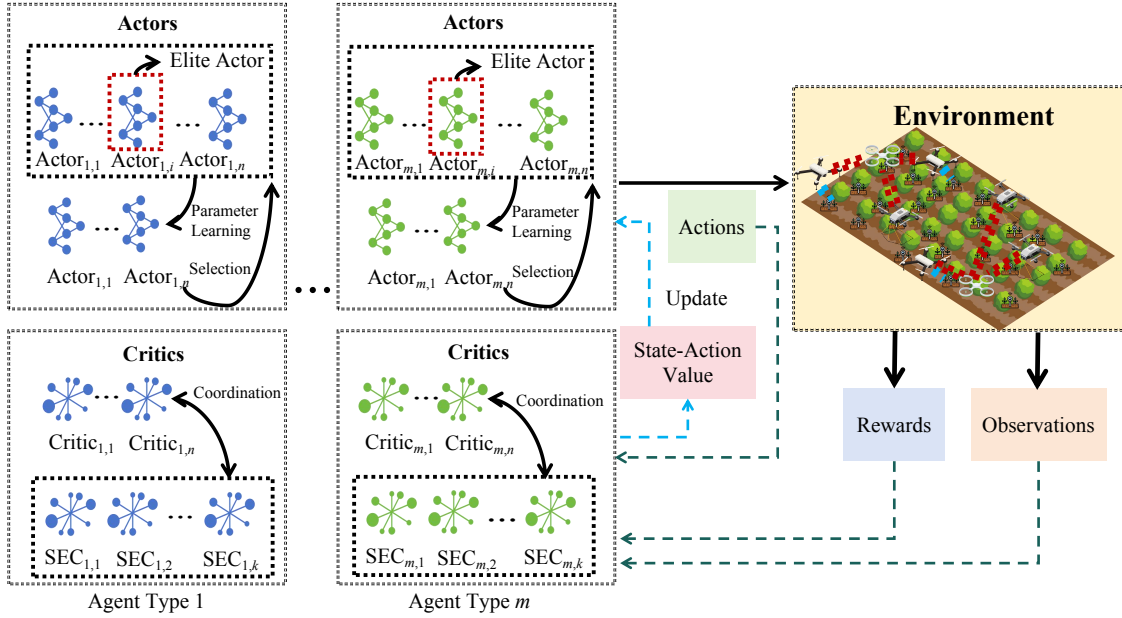


Figure 2: The structure of our EIA-SEC framework.

Assume that o_{v-i} , a_{v-i} , r_{v-i} , and o_{v-i+1} denote the observation, action, reward, and next observation of agent $v-i$, respectively. Let $S_{B,v-i}$ and $A_{B,v-i}$ denote the sampled state and action batches, and \mathcal{D} the replay buffer. We update actor $\mathcal{J}_{\pi_{v-i}}(\theta_{v-i}|A_{B,v-i}, S_{B,v-i})$ by maximizing the sum of the estimated Q-values from the critic $Q_{v-i}(\phi_{v-i}|A_{B,v-i}, S_{B,v-i})$. The loss function $\mathcal{J}_{\pi_{v-i}}(\theta_{v-i})$ can be represented as:

$$\mathcal{J}_{\pi_{v-i}}(\theta_{v-i}) = \mathbb{E}[Q_{v-i}(S_{B,v-i}, \pi_{\theta_{v-i}}(\theta_{v-i}|A_{B,v-i}, S_{B,v-i}))]. \quad (59)$$

5.4 EIA-SEC Framework

As shown in Fig. 2, we combine the EIA and SEC mechanisms with the actor-critic framework of multi-agent reinforcement learning (MARL) for trajectory optimization problems. In our proposed EIA-SEC framework, each agent cooperates with both the same type and different types of other agents. As mentioned in Section 5.2, actors periodically select the advantaged individuals for learning, and generate action policies to interact with the environment. The interaction with environments leads to the rewards and states for critics to evaluate the action-state value of the action policy. As introduced in Section 5.3, agents within the same type, in addition to their own individual critics, are also equipped with SECs, which interact and co-learn with the individual critics. This design helps prevent the overestimation of Q-values and leads to more impartial action-state value evaluations. Moreover, since the SECs are continuously updated through interactions with different agents within the type, they implicitly enable cross-agent critique sharing, thereby accelerating the learning process.

Algorithm 4 The training process of the EIA-SEC.

```

1: Initialize actors  $\pi_{v-i}(\theta_{v-i})$ ,  $v = \{c, m, d\}$ ,  $i = 1, \dots, n_v$ .
2: Initialize critics  $Q_{v-i}(\phi_{v-i})$ ,  $v = \{c, m, d\}$ ,  $i = 1, \dots, n_v$ .
3: Initialize target critics  $Q'_{v-i}(\phi'_{v-i})$  as (58),  $v = \{c, m, d\}$ ,  $i = 1, \dots, n_v$ .
4: Initialize SECs  $Q_{s,v}(\phi_s)$ ,  $v = \{c, m, d\}$ ,  $i = 1, \dots, n_v$ .
5: Reset environment.
6: for episode  $\lambda = 0, 1, \dots, \lambda_{\max}$  do
7:   Update elite imitation strategy as Algorithm 2.
8:   for step  $\lambda' = 0, 1, \dots, \lambda'_{\max}$  do
9:     for  $v = \{c, m, d\}$  do
10:      for agent $v-i$   $i = 1, 2, \dots, n_v$  do
11:        Output action  $\mathbf{a}_{v-i, \lambda'}$  from  $\pi_{v-i}(\theta_{v-i})$ .
12:        Interact with environment, store  $o_{v-i}$ ,  $a_{v-i}$ ,  $r_{v-i}$ , and  $o_{v-i+1}$  to  $\mathcal{D}$ .
13:        Update  $Q_{v-i}(\phi_{v-i})$ ,  $Q'_{v-i}(\phi'_{v-i})$ , and  $Q_{s,v}(\phi_s)$  as Algorithm 3.
14:        Update  $\pi_{v-i}(\theta_{v-i})$  as (60).
15:      end for
16:    end for
17:  end for
18: end for

```

Assume that o_{v-i} , a_{v-i} , r_{v-i} , and o_{v-i+1} denote the observation, action, reward, and next observation of agent _{$v-i$} , respectively. Let $S_{B,v-i}$ and $A_{B,v-i}$ denote the sampled state and action batches, respectively, and \mathcal{D} denote the replay buffer. We update actor $\mathcal{J}_{\pi_{v-i}}(\theta_{v-i}|A_{B,v-i}, S_{B,v-i})$ by maximizing the sum of the estimated Q-values from the critic $Q_{v-i}(\phi_{v-i}|A_{B,v-i}, S_{B,v-i})$. The loss function $\mathcal{J}_{\pi_{v-i}}(\theta_{v-i})$ can be represented as:

$$\mathcal{J}_{\pi_{v-i}}(\theta_{v-i}) = \mathbb{E}[Q_{v-i}(S_{B,v-i}, \pi_{\theta_{v-i}}(\theta_{v-i}|A_{B,v-i}, S_{B,v-i}))]. \quad (60)$$

The training process of EIA-SEC is shown in **Algorithm 4**.

6 Evaluation

6.1 Experimental Setup

We adopt a simulation based on real-world layout³. Tables 1 and 2 present the environmental settings and hyperparameters, respectively. We evaluate the EIA-SEC from four perspectives: training performance, scalability and complexity analysis, ablation study, and 3D visualization. To enhance generalizability, we train the models on 20 different farmland scenarios with different WSN distributions and test them on a random one. We define the following performance metrics:

- Reward (M1): This metric measures the average reward per agent received during one episode.
- Convergence time (M2): This metric measures the number of iterations it takes for the algorithm to converge.
- Stability and Generalization (M3): This metric measures the fluctuations after convergence with the dynamic scenarios.
- Scalability (M4): This metric measures how the inference time per timestep varies with the number of UAVs.
- Policy Efficiency (M5): This metric measures the inference time of UAVs during tasks.

Note that the metrics M1-M3 are measured from the training results, while metrics M4 and M5, as well as UAV trajectories, are obtained from the testing results. We set $n_c = 4$, $n_d = 4$, and $n_m = 4$ except for the scalability study.

6.2 Training Performance

The non-RL algorithms, e.g., heuristics, fail to handle multi-task control in complex and dynamic environments. Therefore, we select three state-of-the-art MARL algorithms as baselines: MASAC [29], MATD3 [30], and MADDPG [28], which are based on the actor-critic framework and can handle continuous action spaces.

³Referring to the intelligent farm layout and UAV data used in the Zhuozhou Teaching Experimental Farm [37].

Table 1: Environmental Parameters for the Agricultural Application [37].

Symbol	Definition	Value	Unit	Symbol	Definition	Value	Unit
$U_{x-\min}$	Task Space Left Edge	0	m	$U_{x-\max}$	Task Space Right Edge	400	m
$U_{y-\min}$	Task Space Back Edge	0	m	$U_{y-\max}$	Task Space Front Edge	400	m
$V_{x-\max}$	x Dire. Maximum Velocity	10	m/s	$V_{y-\max}$	y Dire. Maximum Velocity	10	m/s
H_c	UAV _c Heights	22	m	H_m	UAV _m Heights	20	m
H_d	UAV _d Heights	18	m	n_{WS}	Total WS Number	400	m
n_{px}	x Dire. Plot Number	20	-	n_{py}	y Dire. Plot Number	20	-
AoI_{\max}	Maximum AoI	5	-	VDF_{\max}	Maximum VDF	5	-
ϵ_1	Distance Weight Parameter	0.5	-	ϵ_2	Distance Weight Parameter	0.2	-
ϵ_3	Distance Weight Parameter	0.3	-	m_{UAV}	UAV Mass	0.2	kg
g	Gravitational Acceleration	9.8	-	ρ_{air}	Air Density	1.225	kg/m ³
v_{th}	Hovering Speed Threshold	0.1	m/s	C_d	Viscosity Coefficient	0.5	-
n_{prp}	Propeller Number	4	-	R_{prp}	Propeller Radius	0.1	m
η	Mechanical Efficiency	0.8	-	A_{surf}	UAV Fuselage Area	0.01	m ²
P_{static}	Static Power	4	W	V	Voltage	5	V
f^*	Clock Frequency	$200 \cdot 10^6$	Hz	α^*	Activity Factor	0.5	-
C^*	Load Capacitance	6.4	nF	$T_{update,AoI}$	AoI Updating Time	40,50,60	s
P_{ur}	UAV Received Power	20	dBm	P_{ut}	UAV Transmission Power	20	dBm
P_{cam}	Camera Power	2.5	W	P_{ec}	Extra Communication Power	40	dBm
k_B	Boltzmann Constant	$1.38 \cdot 10^{-23}$	-	T_K	Temperature (Kelvin)	298	K
Bw	Bandwidth	20	MHz	f_c	Signal Frequency	2.8	GHz
I_{type}	WS Type Number	3	-	T_{UA}	AoI Updating Time	40,50,60	s
L	Package Length	20	Bytes	t_{step}	Time Cell	1	s
t_v	VDF Update Cycle	30	s	a_1	Scaling Factor	0.2	-
a_2	Frequency Exponent	0.5	-	a_3	Distance Exponent	0.3	-

Table 2: Hyperparameters for the Agricultural Application.

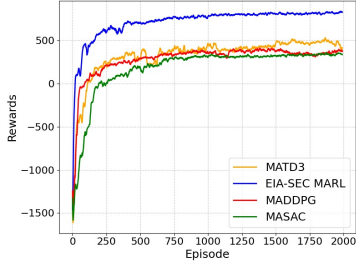
Symbol	Definition	Value	Symbol	Definition	Value
α_1	DPF Parameter	1	α_2	Energy Parameter	0.005
α_3	Collision Risky Penalty	5	α_4	Boundary Violation Penalty	10
α_5	VMUF Parameter	2	α_6	VDF Penalty	0.5
α_7	VDF Motivation	0.2	α_8	DCUF Parameter	2
α_9	AoI Penalty	0.5	α_{10}	AoI Motivation	0.2
γ	Discounted Factor	0.99	ξ	Soft Update parameter	0.005
r_a	Learning Rate for Actor	10^{-4}	r_c	Learning Rate for Critic	10^{-5}
\mathcal{D}	Replay Buffer Size	2^{16}	\mathcal{B}	RL Training Batch Size	128
λ_{\max}	Maximum Training Episode	2000	λ'_{\max}	Maximum Training Step	500
ϑ^*	Update Coefficient	0.1	δ^*	Mimicry Cycle Factor	10
τ	SEC Update Parameter	0.1	ϵ	Rate Parameter	0.1

6.2.1 Evaluation of M1

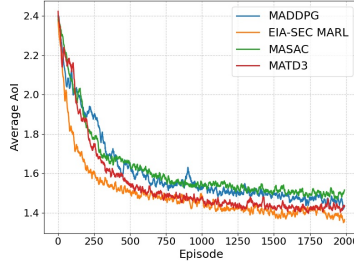
As shown in Fig. 3a, the proposed EIA-SEC achieves significantly higher average rewards than all DRL baselines. This improvement can be attributed to the EIA module, which enhances overall performance by learning from elite individuals and preventing the agents from rapidly converging to local optima. In addition, the SEC component mitigates the overestimation of state-action values, thereby improving the reliability and effectiveness of policy selection. MADDPG, MATD3, and MASAC exhibit similar reward levels, lower than EIA-SEC. As illustrated in Figs. 3b and 3c, EIA-SEC achieves the best performance in both AoI and VDF, significantly outperforming all other baselines. This observation is consistent with the results shown in Fig. 3a, indicating that EIA-SEC can guarantee the timeliness of both data collection and image acquisition.

6.2.2 Evaluation of M2

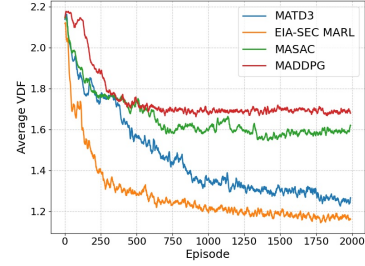
As shown in Fig. 3a, all approaches converge within 800 episodes, while EIA-SEC yields a higher convergence speed. This indicates that the elite selection and learning strategy employed in EIA effectively reduces the agents' learning



(a) Reward performance comparison with other DRL algorithms.



(b) AoI performance comparison with other DRL algorithms.



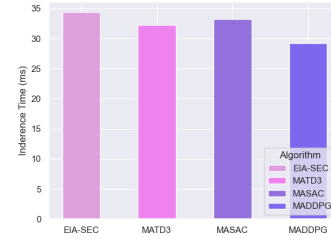
(c) VDF performance comparison with other DRL algorithms.



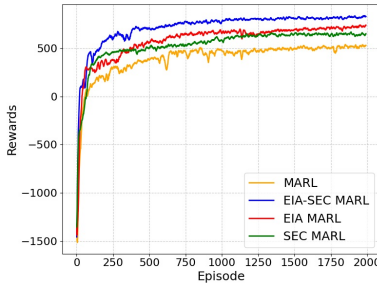
(d) Inference time of EIA-SEC in the scalability study.



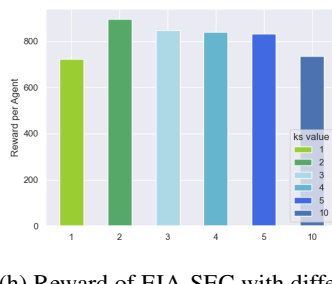
(e) Reward of EIA-SEC in the scalability study.



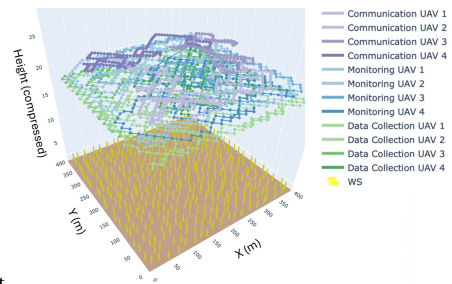
(f) Inference time comparison with other DRL algorithms.



(g) Reward in ablation study.



(h) Reward of EIA-SEC with different k_s .



(i) Visualization of UAV trajectories.

Figure 3: Experimental results in the performance, scalability, ablation, and visualization studies.

and exploration costs, enabling them to escape local optima. Meanwhile, SEC ensures that the critics can learn the state-action value estimations more efficiently, thereby providing more stable and reliable evaluations.

6.2.3 Evaluation of M3

Moreover, the reward curve of EIA-SEC is more stable compared to other baselines. EIA prevents agents from drifting toward non-optimal learning directions and deviating from the optimal policy, while SEC mitigates overestimation of state-action values, thus preventing agents from making inappropriate action decisions.

Therefore, it can be concluded that EIA-SEC achieves best M1 performance, consistently surpassing all the DRL baselines in reward. For M2, EIA-SEC shows faster convergence than other algorithms, yielding higher training efficiency. Furthermore, its M3 metrics exhibit obvious advantages over DRL baselines, showing higher convergence stability.

6.3 Scalability and Complexity Analysis

In this experiment, we first vary the number of the total UAVs n_{UAV} from 6 to 24 to analyze the computational complexity. Then, we set $n_{UAV} = 12$, and compare the inference time of proposed EIA-SEC and other baseline algorithms.

6.3.1 Evaluation of M4

Figs. 3d and 3e illustrate that although the inference time of the proposed EIA-SEC increases with the number of agents, the average reward per agent remains relatively stable. This is because, as the number of agents grows, the algorithm requires additional computation to analyze inter-UAV positional relationships and trajectory decision-making, which increases the inference overhead. Nevertheless, this increase remains within an acceptable range and is much smaller than the UAVs' actual task execution time. Therefore, we conclude that EIA-SEC demonstrates good scalability when the number of UAVs increases.

6.3.2 Evaluation of M5

For inference time, we compare the proposed EIA-SEC with DRL baselines. Fig. 3f shows that the inference time of EIA-SEC is on the same order of magnitude as that of the other DRLs, with MADDPG performing the best. Nevertheless, the performance of MADDPG is much lower than EIA-SEC since it tends to get stuck in local optima, and it is prone to overestimation of state-action values. Furthermore, the introduction of the EIA-SEC module does not lead to a significant increase in inference time. This is because during the offline decision-making phase, EIA does not introduce additional overhead for elite learning, and the computational cost of elite selection and learning is much smaller than that of completing an episode, thus having no impact on inference time. In addition, although the SEC module introduces extra computational cost for state-action value evaluation, the resulting interactions are far less intensive than the overall system overhead of UAV task decision-making. Moreover, since this process occurs during the offline phase, it does not affect online decision-making.

6.4 Ablation Study

We evaluate the effectiveness of the proposed EIA and SEC modules. As shown in Fig. 3g, the inclusion of the EIA and SEC modules significantly enhances the reward performance. This improvement can be attributed to the EIA module, which generates additional experience by selecting and learning from elite individuals. These elite experiences provide valuable guidance to other agents, enabling them to learn more effectively and share strategies across the population. As a result, the agents can reduce the cost of trial-and-error learning, leading to faster convergence, higher reward levels, and greater stability in training. Besides, the SEC module introduces additional critics to help agents estimate state-action values more quickly and efficiently. Through inter-agent negotiation, it also ensures consistency in the evaluation schemes among agents and mitigates value overestimation, thereby improving convergence speed and overall reward performance. Furthermore, we depict the impacts of the SEC structure on the reward performance in Fig. 3h, where k_s -value represents the number of critics in the SEC module. The result shows that a higher k_s -value does not necessarily lead to better reward performance for the agents, and 2 critics in the SEC module yield the best performance in the considered scenario. This is because excessive negotiation and learning from other agents' evaluation strategies can reduce the agents' exploration ability. Therefore, to achieve better overall performance, the k -value should be maintained within a reasonable range. In summary, the EIA and SEC modules play a crucial role in accelerating learning while simultaneously improving both efficiency and robustness of the multi-agent collaborative control.

6.5 Visualization

Fig. 3i shows an exemplary UAV trajectory visualization⁴, which illustrates the collaborative behavior among different types of UAVs. Among them, data collection and monitoring UAVs have more regular shapes to jointly patrol the entire farmland to minimize both AoI and VDF in the intelligent agriculture system, while communication UAVs have more irregular routes among other types of UAVs, serving as auxiliary aerial platforms to provide communication services.

7 Conclusion

We targeted a multi-UAV smart agricultural system, where the UAVs for data collection, image acquisition, and communication tasks work collaboratively. We developed a MARL framework, EIA-SEC, that enhances both decision-making stability and generalization capability for multi-agent systems operating in dynamic and complex environments. Within the context of intelligent agricultural UAV systems, our approach demonstrates improved convergence behavior and superior performance in coordinated sensing and monitoring tasks. Overall, the results indicate that elite-guided policy learning and shared critic ensembles offer a promising direction for advancing MARL in real-world applications.

⁴More visualization results are available at [link to visualization results].

References

- [1] Milandeep Kour Bali and Monika Singh. Farming in the digital age: Ai-infused digital twins for agriculture. In *2024 3rd International Conf. on Sentiment Analysis and Deep Learning (ICSADL)*, pages 14–21, 2024.
- [2] Kai Yan, Linfei Ma, and Yougen Zhang. Research on the application of 5g technology in uav data link. In *2020 IEEE 9th Joint International Information Technology and Artificial Intelligence Conf. (ITAIC)*, volume 9, pages 1115–1118, 2020.
- [3] Dilan Onat Alakuş and Ibrahim Turkoglu. Smart agriculture, precision agriculture, digital twins in agriculture: Similarities and differences. In *2024 Innovations in Intelligent Systems and Applications Conf. (ASYU)*, pages 1–5, 2024.
- [4] Ihsan Ali, Ismail Ahmedy, Abdullah Gani, Muhammad Umair Munir, and Mohammad Hossein Anisi. Data collection in studies on internet of things (iot), wireless sensor networks (wsns), and sensor cloud (sc): Similarities and differences. *IEEE Access*, 10:33909–33931, 2022.
- [5] Gaoyi Ji, Changhai Luo, Lin Cui, Guangqiang Zhang, and Mingxi Shao. Research and testing of remote monitoring system for oil level in agricultural machinery tanks. In *2024 2nd International Conf. on Artificial Intelligence and Automation Control (AIAC)*, pages 267–271, 2024.
- [6] Gemma Hornero, Jordi Llop-Casamada, and Óscar Casas Casas. Capacitive sensor to estimate plant protection products sprayed in precision agriculture applications. In *2024 IEEE International Workshop on Metrology for Industry 4.0 and IoT (MetroInd4.0 and IoT)*, pages 134–138, 2024.
- [7] Rolf A. Kjellby, Linga R. Cenkeramaddi, Anders Frøylog, Baltasar B. Lozano, J. Soumya, and Meghana Bhange. Long-range and self-powered iot devices for agriculture and aquaponics based on multi-hop topology. In *2019 IEEE 5th World Forum on Internet of Things (WF-IoT)*, pages 545–549, 2019.
- [8] Carlos Solon Soares Guimaraes, Maik Basso, Artur Martini da Rosa, Pedro Henrique Morgan Pereira, Edison Pignaton de Freitas, and Carlos E Pereira. Modular architecture for uav cooperation in digital agriculture. In *2025 IEEE Latin Conf. on IoT (LCIoT)*, pages 278–281, 2025.
- [9] Otávio A. R. da Cruz, Lucas U. Haack, Daniel H. Pohren, Alexandre dos S. Roque, Carlos E. Pereira, and Edison P. de Freitas. A holistic communication approach to support uavs and ground sensors in precision agriculture. In *2025 IEEE Latin Conf. on IoT (LCIoT)*, pages 282–285, 2025.
- [10] Henrique C. Oliveira, Vitor C. Guizilini, Israel P. Nunes, and Jefferson R. Souza. Failure detection in row crops from uav images using morphological operators. *IEEE Geoscience and Remote Sensing Letters*, 15(7):991–995, 2018.
- [11] Sandeep Gupta, Jayant Kumar Mohanta, and Ajmal Jaleel. Design of path tracking control and flying ad-hoc network rejoin policy in multi-uav system. In *2023 International Conf. on Control, Communication and Computing (ICCC)*, pages 1–6, 2023.
- [12] Zhenyi Zhu, Yu Qian, and Wei Zhang. Research on uav searching path planning based on improved ant colony optimization algorithm. In *2021 IEEE 3rd International Conf. on Civil Aviation Safety and Information Technology (ICCASIT)*, pages 1319–1323, 2021.
- [13] Kun Jiang, Xiaochen Cao, Wenguang Song, and Qiongqin Jiang. Drl-based multi-dimensional resource scheduling for intelligent connected vehicles in uav-assisted vec systems. *IEEE Sensors Journal*, 2025.
- [14] Jingzhi Bi, Wei Huang, Bei Li, and Lingbo Cui. Research on the application of hybrid particle swarm algorithm in multi-uav mission planning with capacity constraints. In *2024 IEEE International Conf. on Unmanned Systems (ICUS)*, pages 928–933, 2024.
- [15] Xi Chen, Zhe Lin, Haiyan He, Qinglei Hu, and Ruihao Cao. Uav path planning with no-fly-zone constraints by convex optimization. In *2021 40th Chinese Control Conf. (CCC)*, pages 7713–7717, 2021.
- [16] Chang-Sun Yoo, Am Cho, Bum-Jin Park, Young-shin Kang, Sang-Wook Shim, and Il-Hyung Lee. Collision avoidance of smart uav in multiple intruders. In *2012 12th International Conf. on Control, Automation and Systems*, pages 443–447, 2012.
- [17] Yu Ding, Weidang Lu, Yu Zhang, Yunqi Feng, Bo Li, and Yuan Gao. Energy consumption minimization for secure uav-enabled mec networks against active eavesdropping. In *2023 IEEE 98th Vehicular Technology Conf. (VTC2023-Fall)*, pages 1–5, 2023.
- [18] Atakan Yılmaz and Cenk Toker. Air-to-air channel model for uav communications. In *2022 30th Signal Processing and Communications Applications Conf. (SIU)*, pages 1–4, 2022.

- [19] Lei Yang, Haipeng Yao, Xing Zhang, Jingjing Wang, and Yunjie Liu. Multi-uav deployment for mec enhanced iot networks. In *2020 IEEE/CIC International Conf. on Communications in China (ICCC)*, pages 436–441, 2020.
- [20] Praveen Kumar Reddy Maddikunta, Saqib Hakak, Mamoun Alazab, Sweta Bhattacharya, Thippa Reddy Gadekallu, Wazir Zada Khan, and Quoc-Viet Pham. Unmanned aerial vehicles in smart agriculture: Applications, requirements, and challenges. *IEEE Sensors Journal*, 21(16):17608–17619, 2021.
- [21] Xiaoyu Li, Yongrong Sun, and Zhenshu Yang. Uavs-based smart agriculture iot systems: An application-oriented design. In *2023 6th International Symposium on Autonomous Systems (ISAS)*, pages 1–5, 2023.
- [22] Mohammad Akbari, Aisha Syed, W. Sean Kennedy, and Melike Erol-Kantarci. Constrained federated learning for aoi-limited sfc in uav-aided mec for smart agriculture. *IEEE Trans. on Machine Learning in Communications and Networking*, 1:277–295, 2023.
- [23] David Robledo Di Martini, Everton Castelão Tetila, José Marcato Junior, Edson Takashi Matsubara, Henrique Siqueira, Amaury Antônio de Castro Junior, Márcio Santos Araujo, Carlos Henrique Monteiro, Hemerson Pistori, and Veraldo Liesenberg. Machine learning applied to uav imagery in precision agriculture and forest monitoring in brazililian savanah. In *IGARSS 2019 - 2019 IEEE International Geoscience and Remote Sensing Symposium*, pages 9364–9367, 2019.
- [24] Emilian Vlasceanu, Marius Dima, Dan Popescu, and Loretta Ichim. Sensor and communication considerations in uav-wsn based system for precision agriculture. In *2019 IEEE International Conf. on Cybernetics and Intelligent Systems (CIS) and IEEE Conf. on Robotics, Automation and Mechatronics (RAM)*, pages 281–286, 2019.
- [25] Jinyu Zheng, Xiyun Sun, Yuanfa Ji, and Jianhui Wu. Research on uav path planning based on improved aco algorithm. In *2023 IEEE 11th Joint International Information Technology and Artificial Intelligence Conf. (ITAIC)*, volume 11, pages 762–770, 2023.
- [26] Golam Muktader Nayeem, Mingyu Fan, Golam Muktader Daiyan, and Khaled Saifullah Fahad. Uav path planning with an adaptive hybrid pso. In *2023 International Conf. on Information and Communication Technology for Sustainable Development (ICICT4SD)*, pages 139–143, 2023.
- [27] Xi Chen, Zhe Lin, Haiyan He, Qinglei Hu, and Ruihao Cao. Uav path planning with no-fly-zone constraints by convex optimization. In *2021 40th Chinese Control Conf. (CCC)*, pages 7713–7717, 2021.
- [28] Yu Wang, Tianjun Ren, and Zilin Fan. Autonomous maneuver decision of uav based on deep reinforcement learning: Comparison of dqn and ddpg. In *2022 34th Chinese Control and Decision Conf. (CCDC)*, pages 4857–4860, 2022.
- [29] Bhagawat Adhikari, Ahmed Shaharyar Khwaja, Muhammad Jaseemuddin, and Alagan Anpalagan. Sum rate maximization for ris-assisted uav-iot networks using sample efficient sac technique. In *2024 IEEE 10th World Forum on Internet of Things (WF-IoT)*, pages 463–468, 2024.
- [30] Ziyang Zhang, Jie Tian, Di Wang, Jingping Qiao, and Tiantian Li. Td3-based joint uav trajectory and power optimization in uav-assisted d2d secure communication networks. In *2022 IEEE 96th Vehicular Technology Conf. (VTC2022-Fall)*, pages 1–5, 2022.
- [31] Yu Wan, Zipeng Zhao, Jun Tang, Xi Chen, and Jingtao Qi. Multi-uav formation obstacles avoidance path planning based on ppo algorithm. In *2023 9th International Conf. on Big Data and Information Analytics (BigDIA)*, pages 55–62, 2023.
- [32] Jakob Foerster, Gregory Farquhar, Triantafyllos Afouras, Nantas Nardelli, and Shimon Whiteson. Counterfactual multi-agent policy gradients, 2024.
- [33] Zhikai Liu, Navneet Garg, and Tharmalingam Ratnarajah. Dynamic energy efficient resource allocation for massive mimo networks using randomized ensembled double q-learning algorithm. *IEEE Trans. on Cognitive Communications and Networking*, 11(4):2201–2215, 2025.
- [34] Tian Tan, Tianshu Chu, and Jie Wang. Multi-agent bootstrapped deep q-network for large-scale traffic signal control. In *2020 IEEE Conf. on Control Technology and Applications (CCTA)*, pages 358–365, 2020.
- [35] Arezoo Samiei, Sarah Ismail, and Liang Sun. Cluster-based hungarian approach to task allocation for unmanned aerial vehicles. In *2019 IEEE National Aerospace and Electronics Conf. (NAECON)*, pages 148–154, 2019.
- [36] International Telecommunication Union, Radiocommunication Sector (ITU-R). Attenuation in vegetation. Technical Report P.833-9, ITU-R, 2018. Recommendation ITU-R P.833-9.
- [37] CAU Zhuozhou Teaching Experimental Farm contributors. China Agricultural University Zhuozhou Teaching Experimental Farm (Agricultural Science Park). <https://zzkj.cau.edu.cn/col/col131926/index.html>, 2025. access on 24 November 2025.